CrossMark

Mechanical Response of Borosilicate and Soda-Lime Glass Under Dynamic Triaxial Compression

John T. Chojnacki[1] · Weinong W. Chen[1]

Abstract Dynamic triaxial compression experiments were performed on borosilicate and soda-lime glass using a triaxial compression Kolsky bar that has two pressure chambers, one enclosing the specimen and the other enclosing the end of the transmission bar. A specimen is pre-stressed hydrostatically before being loaded by a dynamic axial stress wave. Specimen axial stress and strain are determined at high strain rates under a range of hydrostatic pressures. Borosilicate glass was subjected to pressures of 25, 50, and 100 MPa at a strain rate of $1500\ s^{-1}$, and soda-lime glass was subjected to 25, 50, and 75 MPa at $1100\ s^{-1}$. Dynamic results were compared to high-rate unconfined experiments, as well as low-rate confined experiments. It was observed that confined glass strength did not show clear strain-rate dependency. But confining pressure increased the glass strength.

Keywords Kolsky bar (SHPB) · Triaxial · Glass · Borosilicate · Soda-lime

Introduction

Glass has been widely used in layered transparent vehicle armors where the glass material is subjected to high-rate, multiaxial compression loading. It is desired to determine the mechanical response of glass under such loading conditions. However, due to the limitations in experimental techniques, there have been a few studies on the high-rate compressive response of glass under multiaxial compression. The method to simulate multiaxial compression was mainly through mechanical confining jackets. For example, Xu and Chen [1] studied the effects of loading rate, temperature, and damage effects on the compressive response of a borosilicate glass confined in sleeves of different materials. Chocron et al. [2–5] investigated the effects of damage on the strength of a borosilicate (Borofloat 33 manufactured by Schott Glass) and a soda-lime glass (Starphire manufactured by PPG) under confinement. They used thermo-shocks to create initial damage in the glass specimens and then subject the specimens to quasi-static triaxial loading. At high rates, the damaged cylindrical specimens are confined in metal jackets and subjected to axial compressive loading from a Kolsky bar.

Under quasi-static triaxial loading [6], the lateral surface of a cylindrical specimen is subjected to pressure boundary condition. At Kolsky bar rates, cylindrical surface is confined by a metallic cylindrical wall [7], resulting in a mixed pressure/elastic boundary condition. To identify the rate effects on the material response, it is necessary to unify the boundary conditions on the specimen. Since it is difficult to delineate the effects of confinement and friction at the specimen/wall interface in the metal sleeve configuration, it is desired to achieve dynamic triaxial loading conditions during the Kolsky bar experiments. For this purpose, a dynamic triaxial Kolsky bar has been developed [8, 9]. In this device, a compression experiment is performed in two stages. First, a pre-determined hydrostatic pressure is applied on the specimen in the testing section of a Kolsky bar, which is inside a pressure chamber. A dynamic axial stress wave loading is then applied to the specimen by the Kolsky bar. The method has been employed to explore the dynamic triaxial behavior of sand [10] and rock [11]. In this paper, this dynamic triaxial experimental setup is used

✉ Weinong W. Chen
wchen@purdue.edu

[1] Schools of Aero/Astro and Materials Engineering, Purdue University, West Lafayette, IN 47907, USA

252

J. dynamic behavior mater. (2016) 2:251–258

to characterize the dynamic triaxial response of a borosilicate and soda-lime glass.

Materials and Specimens

The two glass materials experimented upon are a borosilicate glass named Borofloat 33 from Schott Inc. in Elmsford, NY, and a soda-lime glass named Starphire from PPG Industries in Pittsburgh, PA. The chemical composition and some physical and material properties are listed in Tables 1 and 2, respectively. Both borosilicate and soda-lime glass materials are commonly used in layered transparent armors and thus have been the subject of investigations. Recent advances on the study of the mechanical behavior of these materials are summarized in a special journal issue [12, 13].

The glass supply came in the form of flat panels. The borosilicate panels had a thickness of 6.53 mm and the soda-lime panels 5.67 mm. Cylindrical specimens were core-drilled out and then ground. The diameter of the cylindrical specimens for both materials was 4.75 mm. The two flat ends of the each cylinder were the original flat surfaces of the panels, ensuring the parallelism of the loading surfaces. Specimens were inspected, weighed, and measured before each experiment to ensure consistency.

Experimental Setup

The experimental setup used in this study was a Kolsky bar integrated with a hydrostatic pressure system which enabled dynamic triaxial compression (DTXC) experiments [8, 9]. A schematic of the experimental setup is shown in Fig. 1 [8], and a photograph of the setup is shown in Fig. 2.

In this system, a specimen is placed between the incident and transmission bars, but is additionally sealed within a radial compression chamber. A second vessel, called the axial compression chamber, is connected to the same pressure line as the radial compression chamber and contains the end of the transmission bar in order to confine specimens axially. As a result, the axial compression chamber replaces the usual momentum bar and shock absorber. The fluid within the axial compression chamber restricts forward motion of the transmission bar during an experiment.

Table 2 Mechanical properties of Borofloat (borosilicate) and Starphire (soda-lime) glass [13]

	ρ (kg cm^{-3})	E (GPa)	υ	σ_{fs} (MPa)
Borofloat 33	2200	64	0.20	25
Starphire	2510	73.1	0.22	41.4

The pressure is controlled at a hydraulic pump by a computer according to predetermined profiles. Pressure from the hydraulic pump is amplified by a piston inside the intensifier, which pressurizes the axial and radial chambers simultaneously. A pressure transducer connected to the intensifier reports the pressure back to the computer for pressure profile control. The axial and radial chambers were proof tested at 500 MPa, and the intensifier was proof tested at 518 MPa. The hydraulic pump has a maximum working pressure of 13.8 MPa, and the intensifier, which amplifies the pressure from the hydraulic pump by a factor of 32, has a maximum working pressure of 440 MPa. The hydraulic pump pressurizes hydraulic oil; however, the output side of the intensifier uses an 80 %/20 % mixture of kerosene and 10 W-30 motor oil.

Pressurizing the axial and radial chambers compresses the incident and transmission bars in addition to the specimen, requiring the addition of the tie rods and restraining plate seen in Figs. 1 and 2. A hole through the restraining plate with a widened recess for a stopper on the incident bar side allows a compression stress wave to pass from the pre-incident bar though the stopper to the incident bar, without the incident bar sliding backward while confined. Having this pre-incident bar also facilitates easier alignment with the striker in the gas gun. Not pictured in Fig. 2 are platens, which are thin discs placed on each side of the specimen between the specimen-bar interfaces. Platens endure the scratches and dings from specimen failure that would otherwise damage the bar surfaces, and are easier to surface grind or replace.

The striker, pre-incident bar, incident bar, transmission bar, and platens all have a diameter of about 18.97 mm, with lengths of 305, 165, 2103, 1191, and 3.05 mm, respectively. The stopper has a diameter of 45.7 mm and a thickness of 25.4 mm. The confining pressure was varied at 25, 50, and 100 MPa for the borosilicate glass, and 25, 50, and 75 MPa for the soda-lime glass. The experimental equipment is capable of achieving higher hydrostatic

Table 1 Percent composition of Borofloat (borosilicate) and Starphire (soda-lime) glass [13]

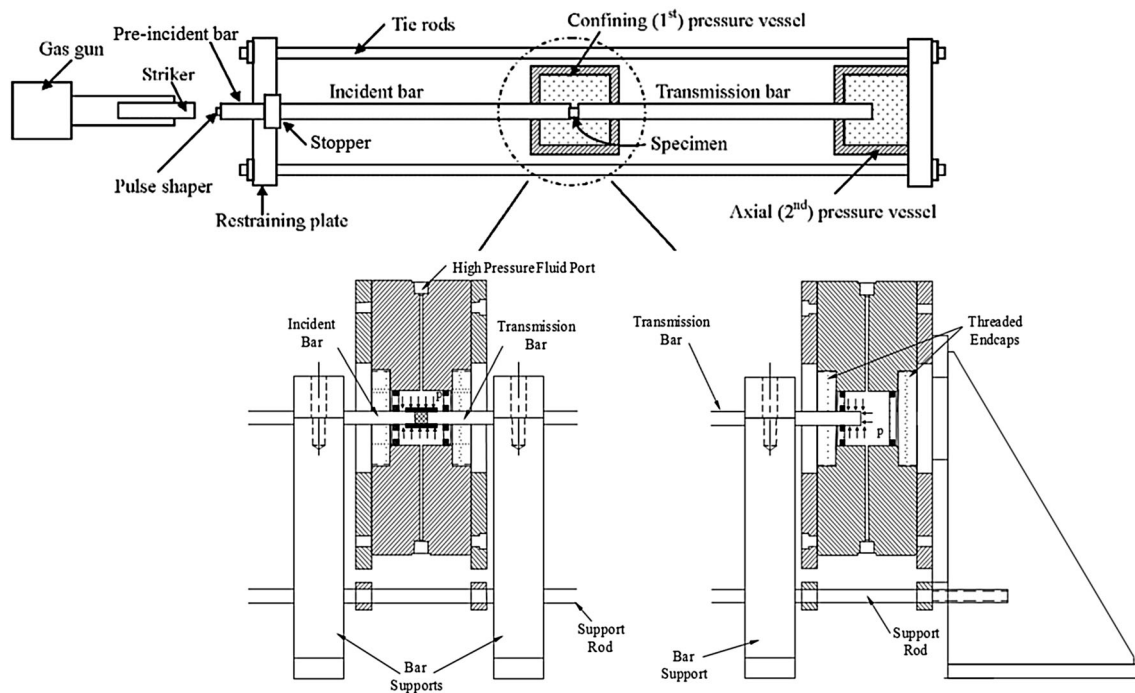|	SiO$_2$	B$_2$O$_3$	Na$_2$O	Al$_2$O$_3$	K$_2$O	CaO	Fe$_2$O$_3$	MgO	SrO	ZrO$_2$
Borofloat 33	80.54	12.7	3.54	2.54	0.64	0.02	0.015	<0.01	–	–
Starphire	73.2	–	14.7	1.44	0.01	10.3	0.01	0.08	0.2	0.03

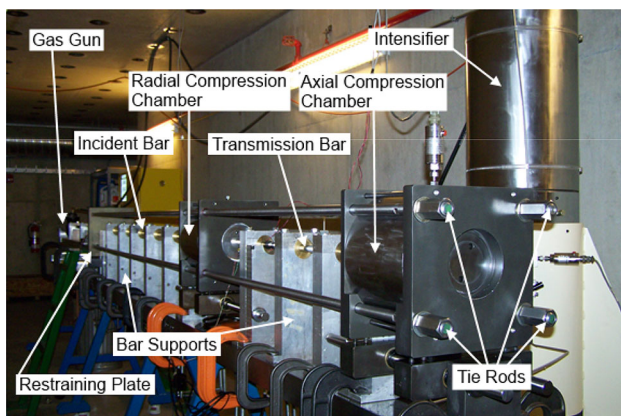**Fig. 1** A schematic of a triaxial compression Kolsky bar [8]

Fig. 2 Labeled image of the triaxial compression Kolsky bar

pressure (up to 400 MPa). However, under the axial impact conditions to achieve the consistent strain rate, the glass specimens did not fail under higher hydrostatic pressures. We report only the data when failure in the glass samples was observed under the confining pressures up to 100 MPa.

The experiments reported in this paper are performed in the strain-rate range that are typically achieved in a Kolsky bar set up ($\sim 10^3$ s^{-1}). To explore the mechanical response of glass under impact loading conditions, experiments at higher strain rates and higher pressure, such as those recently performed by Chocron et al. [14], are also desired to develop insights to the glass failure over a wider range of loading conditions.

Experimental Procedure

In the dynamic triaxial experiments, it is critically important to seal the specimen from the fluid around it. The majority of experiments performed on the triaxial compression Kolsky bar have been specimens with about the same diameter as the incident and transmission bars [10]. To seal these specimens, a piece of heat shrink tubing would be heated and shrunk to fit securely over the length of the specimen and platens. After this, the cut out neck of a balloon would be rolled over the heat shrink tubing, followed by an application of M-Coat B-1 nitrile rubber coating that required 2 h to dry before proceeding with an experiment. The heat shrink tubing, balloon neck, and nitrile rubber coating together provide sufficient protection for the specimen against the fluid that fills the radial confinement chamber, while also preventing fluid from getting in between the specimen-bar interface. A picture of a specimen prepared in this manner is shown in Fig. 3.

This sealing method presents a challenge for specimens much smaller than the bar, particularly the glass specimens, as these protective layers become ineffective at keeping fluid out of the bar-specimen interface. Proper sealing that separates the specimen from the pressure fluid is critical to obtain valid results from the experiments. If the fluid penetrates the seal, the fluid will get in between the specimen and bar interfaces, which changes the boundary conditions assumed on the specimen during the experiment. Also, the fluid will penetrate into the openings in the

254

J. dynamic behavior mater. (2016) 2:251–258

Fig. 3 A sealed acrylic specimen ready for an experiment

specimen created by the damage as the specimen is loaded up, changing the material response significantly through lubrication. Various attempts were made to remedy this situation. The solution eventually settled upon was to wrap the glass specimen in a heat shrink tube that was shrunk and cut to the length of the specimen. Then the specimen was placed between the platens. A seal around the specimen and platens was formed using J-B WaterWeld epoxy. The heat shrink tube was used to help the putty cling to the specimen, and the epoxy putty required an hour to cure after applying it. Figure 4 shows a glass specimen before and after the seal was applied. With the specimen sealed, the experiment proceeds by sliding the radial chamber forward so that the specimen is in the middle of the chamber, and screwing the door closed. Care is taken to not allow the incident bar to rotate during this operation, which would likely break the seal.

For the hydrostatic portion of the experiment, a linear variable differential transformer (LVDT) is attached to the incident and transmission bars just outside the radial chamber to measure the relative motion of the bars between these two points. The motion between these two attachment points subtracted by the elastic deformation of the bars inside the radial chamber gives the relative motion between the bar ends in contact with the specimen [10]. A data-collecting oscilloscope is set to collect data continuously. The axial and radial chambers are filled with the kerosene and motor oil mixture, air bubbles are bled from the top port of each chamber, and the ports are bolted closed. The confinement pressure is increased to the desired level for the experiment. At this point, a glance at the LVDT data will indicate whether axial confinement was successful or not. If the voltage change recorded from the LVDT shows expansion in the specimen rather than compression, then the seal has broken and fluid has leaked into the specimen-
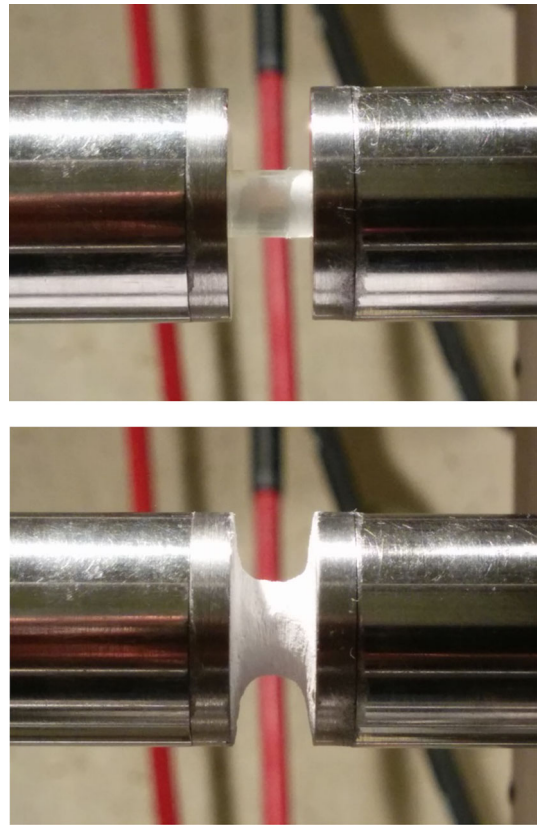

Fig. 4 Glass specimen before (top) and after (bottom) being sealed with WaterWeld

bar interface. Continuing the experiment from this point would not yield any useful results. If the seal appears to still be intact, then the pressure and LVDT data are recorded, the LVDT removed, and the experiment is ready to proceed to the dynamic portion.

For the dynamic portion of the experiment, the strain gages from the incident and transmission bars are reconnected and their signals zeroed. The oscilloscope is set to a single sequence trigger from the incident strain gage. The confinement pressure is verified and the gas gun is fired at the desired pressure in order to finally load the specimen at a high strain rate. Strain gage data from the oscilloscope is saved for later analysis. A half-hardened Cu 110 17.5 mm in diameter, 0.5-mm thick pulse shaper was placed on the front of the pre-incident bar with high pressure grease in the majority of the glass experiments reported in this paper. After the experiment is completed, the hydraulic pump is turned off, and any valves that were closed are reopened to relieve pressure. Fluid from the radial and axial chambers is drained into a waste container, the door to the radial chamber is opened, the remains of the specimen are saved if it is recoverable, and the area is cleaned in preparation for the next experiment.

During an experiment, the confinement pressure, LVDT, and strain gage data are collected using a digital oscilloscope. Figure 5 shows an example of the data collected during an experiment on borosilicate with an initial 50-MPa hydrostatic confinement, after it is passed through a 9 point moving average filter and converted from voltage into the appropriate units. Note that the upper two graphs correspond to the hydrostatic phase where the specimen is slowly pressured; the bottom graph corresponds to the dynamic phase where the striker creates a compressive wave to break the specimen. The incident, reflected and transmitted waves are used to verify that the specimen is in dynamic equilibrium during the dynamic phase of the experiment using a one-wave, two-wave method [15].

Figure 6 shows the strain rate history and stress versus strain graphs obtained from the experiment on borosilicate. During the experiment, the strain rate ramps up and levels out at a somewhat constant level of 1500 s^{-1} before rapidly increasing to indicate failure in the specimen. The principal stress difference increases to about 3000 MPa before the specimen completely fails. Note that this stress value does not account for the initial 50 MPa of axial and radial confinement applied to the specimen. After the unstable region at the specimen failure on the stress–strain curve in Fig. 6, the specimen resume some capacity of resisting axial load at a level of slightly below 1000 MPa as the axial strain further increases. This is the result of the broken specimen being contained inside the sealed enclosure.
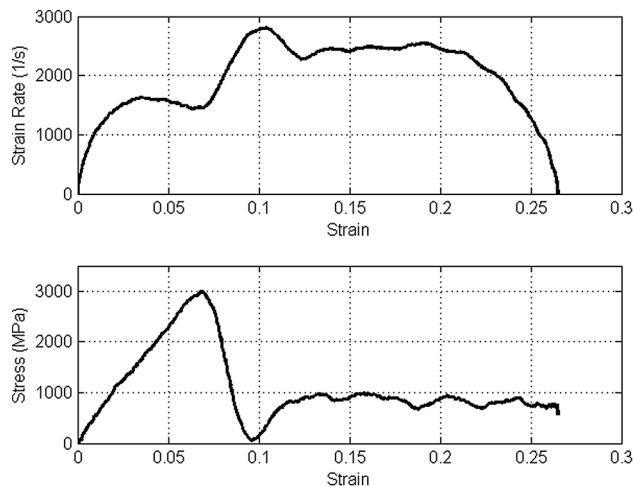

Fig. 6 Strain rate history (top) and stress–strain curve (bottom) for borosilicate glass

Experimental Results

Borosilicate Glass

Table 3 summarizes the confinement pressure P_c, impact velocity of the striker v_s, pulse shaper used, average dynamic stain rate $\dot{\varepsilon}$, and principal stress difference at failure σ_{eq}, for experiments conducted on the borosilicate glass. Figure 7 shows the dependence of σ_{eq} on the confining pressure P_c.

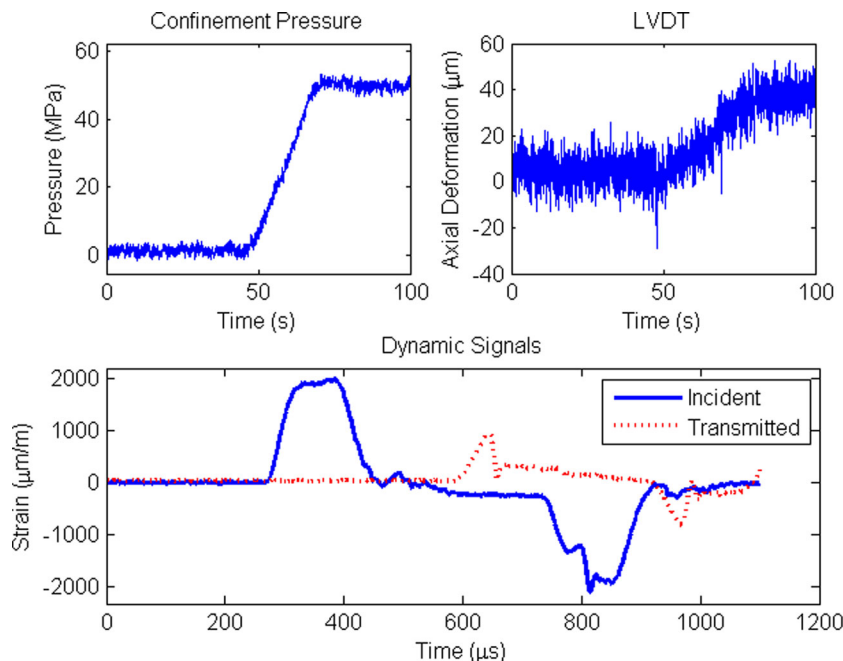Fig. 5 Smoothed and converted data for confinement pressure (top left), LVDT (top right), and strain gages (bottom)

256

J. dynamic behavior mater. (2016) 2:251–258

Table 3 Summary of experiments conducted on borosilicate glass

Sample #	P_c (MPa)	V_s (m s^{-1})	Pulse shaper (in)	$\dot{\varepsilon}$ (s^{-1})	σ_{eq} (MPa)
44	–	–	–	0.001	1889
45	–	–	–	0.001	1571
46	–	–	–	0.001	1592
34	–	21	Cu 110 (11/16,0.02)	∼1800	1903
35	–	17	Cu 110 (11/16,0.02)	∼1400	2004
36	–	15	Cu 110 (11/16,0.02)	∼1300	1813
37	–	14	Cu 110 (11/16,0.02)	∼1200	1924
39	–	15	Cu 110 (11/16,0.02)	∼1300	1962
24	25	21	Cu 110 (11/16,0.02)	∼1650	2862
25	25	21	Cu 110 (11/16,0.02)	∼1650	2989
26	25	21	Cu 110 (11/16,0.02)	∼1600	3069
40	25	21	Cu 110 (11/16,0.02)	∼1600	3072
21	50	21	Cu 110 (11/16,0.02)	∼1500	2883
27	50	21	Cu 110 (11/16,0.02)	∼1550	2779
33	50	21	Cu 110 (11/16,0.02)	∼1500	3001
42	50	21	Cu 110 (11/16,0.02)	∼1500	3005
28	100	21	Cu 110 (11/16,0.02)	∼1450	2789
29	100	21	Cu 110 (11/16,0.02)	∼1400	2965
31	100	21	Cu 110 (11/16,0.02)	∼1400	2784
43	100	21	Cu 110 (11/16,0.02)	∼1350	2954

The results along the vertical axis (zero confining pressure) in Fig. 7 indicate that the unconfined compression experiments at both quasi-static and dynamic rates do not show significant rate effects on the compressive strength. However, there is a notable increase in strength from unconfined to confined experiments, but there is a negligible change in strength over the range of confinement pressures achieved in the experiments conducted in this research.

Soda-Lime Glass

Similar to Table 3, Table 4 summarizes the confinement pressure P_c, impact velocity of the striker v_s, pulse shaper used, average stain rate $\dot{\varepsilon}$, and principal stress difference at

Fig. 7 Variation of principal stress difference at failure as a function of confinement pressure for borosilicate glass

failure σ_{eq}, for experiments conducted on the soda-lime glass. It is noticed that the striking conditions are different from those listed in Table 3. This is the result of the attempts to achieve similar constant strain rates where the striking velocities and pulse shapers are adjusted. Figure 8 shows the variation of σ_{eq} as a function of P_c.

A comparison of the results presented in Figs. 7 and 8 indicates that the soda-lime glass has an overall lower strength than borosilicate glass, but the dependence of strength on pressure shares similar trends. There appears to be no significant rate dependence on strength from the unconfined experiments. There is a notable jump in strength from unconfined to confined experiments, but there is a negligible change in strength over the range of confinement pressures observed.

To compare these experimental results with the quasi-static results in literature, we replotted the borosilicate and soda-lime glass results by Chocron et al. [3, 4], in Figs. 9 and 10, respectively, which are in the form of equivalent stress versus hydrostatic pressure. As a baseline check, we also performed unconfined quasi-static experiments using an MTS. To include the dynamic experimental results reported in Figs. 7 and 8, hydrostatic pressure can be rewritten as $P = P_c + \frac{1}{3}\sigma_{eq}$, where P_c is the fluid confinement pressure applied axially and radially, and σ_{eq} is the principal stress difference at failure. Figure 9 shows σ_{eq} as a function of P for dynamic compression, dynamic triaxial compression, and quasi-static MTS experiments in comparison to Chocron et al. [3] for borosilicate glass. The
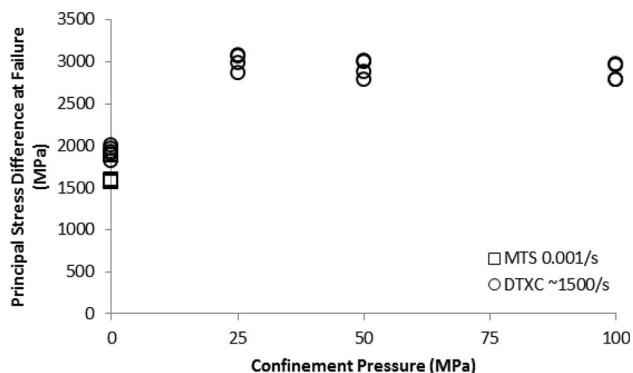
Table 4 Summary of experiments conducted on soda-lime glass

| Sample #	P_c (MPa)	V_s (m s^{-1})	Pulse shaper (in)	$\dot{\varepsilon}$ (s^{-1})	σ_{eq} (MPa)
22	–	–	–	0.001	1178
23	–	–	–	0.001	1115
24	–	–	–	0.001	1218
18	–	10	Cu 110 (11/16,0.02)	∼1100	1153
19	–	10	Cu 110 (11/16,0.02)	∼1100	1229
20	–	10	Cu 110 (11/16,0.02)	∼1050	1285
21	–	10	Cu 110 (11/16,0.02)	∼1050	1238
10	25	12	Cu 110 (11/16,0.02)	∼1100	1715
11	25	15	Cu 110 (11/16,0.03)	∼900	1884
12	25	17	Cu 110 (11/16,0.03)	∼1000	1742
7	50	15	Cu 110 (11/16,0.02)	∼1100	2008
8	50	15	Cu 110 (11/16,0.02)	∼1100	1917
9	50	15	Cu 110 (11/16,0.02)	∼1100	1842
4	75	15	Cu 110 (11/16,0.02)	∼950	1773
13	75	15	Cu 110 (11/16,0.02)	∼1100	1803
14	75	15	Cu 110 (11/16,0.02)	∼1100	1809
17	75	15	Cu 110 (11/16,0.02)	∼1100	1890
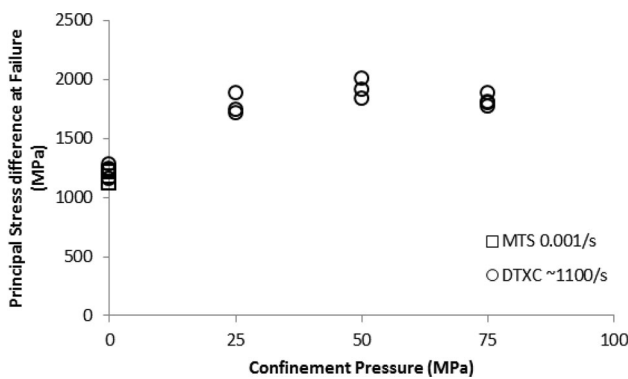
Fig. 8 Variation of principal stress difference at failure with confinement pressure for the soda-lime glass
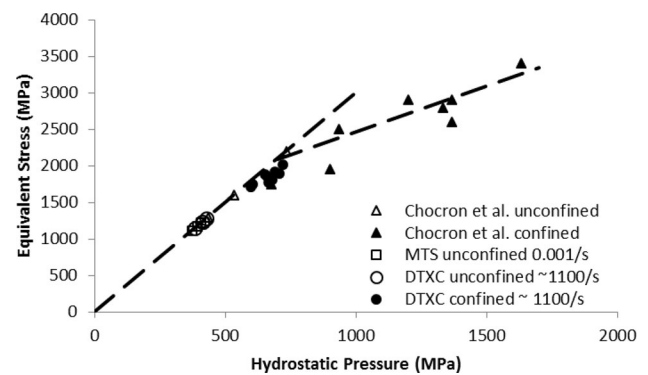

Fig. 10 Comparison of soda-lime specimens tested under triaxial compression, dynamic triaxial compression, and with an MTS [4]
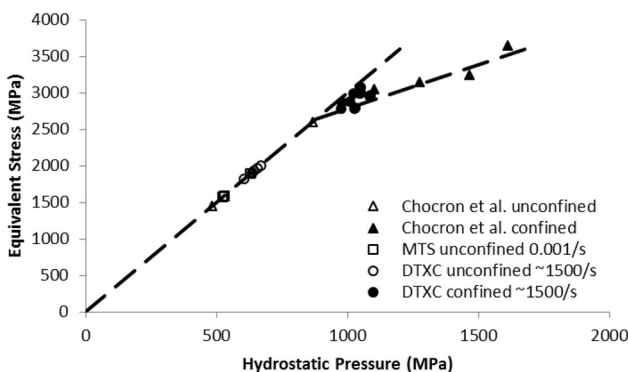

Fig. 9 Comparison of borosilicate specimens tested under triaxial compression, dynamic triaxial compression, and with an MTS [3]

results show that dynamic triaxial compression experiments conducted in this research yield results that agree well with the published results obtained quasi-statically. The quasi-static MTS results also fall on the same curve. These facts clearly indicate that the borosilicate glass is not sensitive to strain rate, especially under the confinement achieved in the reported experiments.

Similarly, Fig. 10 shows the variation of σ_{eq} as a function of P from dynamic compression, dynamic triaxial compression, and MTS experiments in comparison to Chocron et al. [4] for the soda-lime glass. As shown in Fig. 10, the observations made about borosilicate glass also apply to the soda-lime glass, although the average failure strength obtained by the DTXC method for the soda-lime

glass was slightly lower than the trend reported in literature.

The experimental results presented in this paper were obtained at the typical Kolsky bar strain-rate range ($\sim 10^3$ s^{-1}). Experimental results at higher strain rates are still very limited, e,g., Chocron et al. [14], to compare the results over a very wide range of strain rates. However, there have been more studies on the rate and confinement effects on brittle materials such as ceramics. For example, Lankford et al. [16] argued that, as the strain rate is increased from quasi-static to plate-impact ($>10^5$ s^{-1}), the compressive strength of the brittle specimen material should increase gradually with increasing strain rate over the quasi-static rates, and then increase rapidly with rates over the Kolsky-bar rate range. As the rate is further increased, the "uniaxial stress" compressive strength should eventually coincide with the compressive strength obtained from plate-impact experiments under uniaxial strain conditions.

Conclusions

Compression experiments were performed on a borosilicate and a soda-lime glass at a quasi-static strain rate (0.001 s^{-1}) using an MTS, and at a high strain rate (~ 1500 s^{-1} for borosilicate, ~ 1100 s^{-1} for soda-lime) using a modified triaxial compression Kolsky bar. Experiments on the Kolsky bar were performed unconfined and triaxially confined to 25, 50, and 100 MPa for borosilicate glass, and 25, 50, and 75 MPa for soda-lime glass. The dynamic strength of both glass materials increased significantly from unconfined to confined experiments. However, the strength did not further increase with increasing confining pressures achieved in this research. The results of the dynamic triaxial compression experiments performed in this study agree well with the quasi-static triaxial compression results found in literature, indicating minimum strain rate effects for the two glass materials under triaxial loading conditions.

References

1. Nie X, Chen W (2013) High-rate progressive failure of borosilicate glass under mechanical confinement at high temperatures. Exp Mech 53:67–75
2. Chocron S, Dannemann K, Walker J, Nicholls A, Anderson C (2007) Constitutive model for damaged borosilicate glass under confinement. J Am Ceram Soc 90(8):2549–2555
3. Chocron S, Anderson C, Nicholls A, Dannemann K (2010) Characterization of confined intact and damaged borosilicate glass. J Am Ceram Soc 93(10):3390–3398
4. Chocron S, Anderson C, Dannemann E, Nicholls K (2013) Pressure effects on the compressive response of confined intact and damaged soda-lime glass. Exp Mech 53(1):77–89
5. Dannemann K, Anderson C, Chocron S, Spencer J (2012) Damage development in confined borosilicate and soda-lime glasses. J Am Ceram Soc 95(2):721–729
6. Akers SA, Reed PA, Ehrgott JQ (1986) WES high-pressure uniaxial strain and triaxial shear test equipment. Miscellaneous Paper SL-86-11, U.S. Army Engineers, Waterways Experiment Station, Vicksburg, MS
7. Bhushan B, Jahsman WE (1978) Measurement of dynamic material behavior under nearly uniaxial strain conditions. Int J Solids Struct 14:739–753
8. Frew D, Akers S, Chen W, Green M (2010) Development of a dynamic triaxial kolsky bar. Meas Sci Technol 21:105704
9. Kabir M, Chen W (2009) Measurement of specimen dimensions and dynamic pressure in dynamic triaxial experiments. Rev Sci Instrum 80(12):125111
10. Martin B, Kabir ME, Chen W (2013) Undrained high-pressure and high strain-rate response of dry sand under triaxial loading. Int J Impact Eng 54:51–63
11. Hokka M, Black J, Tkalich D, Fourmeau M, Kane A, Hoang N-H, Li CC, Chen WW, Kuokkala V-T (2016) Effects of strain rate and confining pressure on the compressive behavior of kuru granite. Int J Impact Eng 91:183–193
12. Talladay TG, Templeton DW (2014) Glass armor—an overview. Int J Appl Glass Sci 5(4):331–333
13. Parab ND, Black JT, Claus B, Hudspeth M, Sun J, Fezzaa K, Chen W (2014) Observation of crack propagation in glass using X-ray phase contrast imaging. Int J Appl Glass Sci 5(4):363–373
14. Chocron S, Barnette DD, Holmquist TJ, Anderson CE, Bigger RP, Moore TZ (2016) Damage threshold of borosilicate glass under plate impact. J Dyn Behav Mater. doi:10.1007/s40870-016-0056-4
15. Chen W, Song B (2011) Split Hopkinson (Kolsky) bar design, testing and applications (Mechanical engineering series). Springer, New York
16. Lankford J, Anderson CE, Nagy AJ, Walker JD, Nicholas AE, Page RA (1998) Inelastic response of confined aluminum oxide under dynamic loading conditions. J Mater Sci 33:1619–1625